AFRL-VS-TR-2003-1557

ANALYTIC MODELS FOR SUNLIGHT CHARGING OF A RAPIDLY SPINNING SATELLITE

Maurice F. Tautz

Radex, Inc.
Three Preston Court
Bedford, MA 01730

24 January 2003
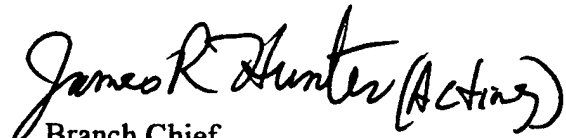
Scientific Report No. 7

20030915 109

AIR FORCE RESEARCH LABORATORY
Space Vehicles Directorate
29 Randolph Rd
AIR FORCE MATERIEL COMMAND
Hanscom AFB, MA 01731-3010

This technical report has been reviewed and is approved for publication.

Contract Manager

Branch Chief

REPORT DOCUMENTATION PAGE

Public reporting burden for this collection of information is estimated to average 1 hour per response, including the time for reviewing instructions, searching existing data sources, gathering and maintaining the data needed, and completing and reviewing the collection of information. Send comments regarding this burden estimate or any other aspect of this collection of information, including suggestions for reducing this burden, to Washington Headquarters Services, Directorate for Information Operations and Reports, 1215 Jefferson Davis Highway, Suite 1204, Arlington, VA 22202-4302, and to the Office of Management and Budget, Paperwork Reduction Project (0704-0188), Washington, DC 20503.

1. AGENCY USE ONLY (Leave Blank)	2. REPORT DATE 24 January 2003	3. REPORT TYPE AND DATES COVERED Scientific Report No. 7

4. TITLE AND SUBTITLE Analytic Models for Sunlight Charging of a Rapidly Spinning Satellite	5. FUNDING NUMBERS PE 61102 F PR S321 TA GY WU AG Contract F19629-98-C-0054
6. AUTHORS Maurice F. Tautz	

7. PERFORMING ORGANIZATION NAME(S) AND ADDRESS(ES) Radex, Inc. Three Preston Court Bedford, MA 01730	8. PERFORMING ORGANIZATION REPORT NUMBER RXR-03-0101

9. SPONSORING / MONITORING AGENCY NAME(S) AND ADDRESS(ES) Air Force Research Laboratory/VSBX 29 Randolph Road Hanscom AFB, MA 01731-3010 Contract Manager: Alan Rebello/VSBX	10. SPONSORING / MONITORING AGENCY REPORT NUMBER AFRL-VS-TR-2003-1557

11. SUPPLEMENTARY NOTES

12a. DISTRIBUTION / AVAILABILITY STATEMENT Approved for Public Release; Distribution Unlimited	12b. DISTRIBUTION CODE

13. ABSTRACT (Maximum 200 words)

A satellite in sunlight can charge to substantial negative voltages, even though the photoelectron surface current is typically much larger than the ambient currents in space, because escaping photoelectrons can be blocked by local potential barriers. In this report, we discuss two analytic models for sunlight charging of a rapidly spinning spherical satellite, both of which are based on blocked photoelectron currents: the monopole-dipole model where the spin axis points at the sun and the monopole-quadrupole model where the sun is perpendicular to the spin axis. A comparison is made between the calculated ratio between the maximum and minimum potentials on the surface and measured ratios for eclipse to sunlight charging obtained from satellites in geosynchronous orbit.

14. SUBJECT TERMS Sunlight charging, Spinning, Blocked photoelectrons, Satellites		15. NUMBER OF PAGES
		16. PRICE CODE

17. SECURITY CLASSIFICATION OF REPORT Unclassified	18. SECURITY CLASSIFICATION OF THIS PAGE Unclassified	19. SECURITY CLASSIFICATION OF ABSTRACT Unclassified	20. LIMITATION OF ABSTRACT Unlimited

NSN 7540-01-280-5500

Standard Form 298 (Rev. 2-89)
Prescribed by ANSI Std. Z39-1
298-102

CONTENTS

LIST OF FIGURES

ACKNOWLEDGMENTS

1. INTRODUCTION

It is well known that a satellite in sunlight can charge to substantial negative voltages, even though the photoelectron current (positive) is typically much larger than the ambient currents in space. This effect o ccurs b ecause e scaping photoelectrons c an b e b locked b y l ocal p otential b arriers. T he formation of such a barrier is a multidimensional effect, where surfaces of high negative potential suppress the escape of low energy electrons elsewhere on the satellite. When the outgoing flux of photoelectrons is reduced in this way, current balance on the satellite can be readily achieved. In this report, we consider two analytic models for sunlight charging of a rapidly spinning spherical satellite, both of which are based on blocked photoelectron currents:

1)   The Sun is situated on the spin axis of the satellite.
        This is the monopole-dipole (MD) model.

2)   The Sun is perpendicular to the spin axis of the satellite.
        This is the monopole-quadrupole (MQ) model.

The first model, MD, where the satellite may be non-rotating, has been treated by *Besse and Rubin* [1980] and others [*Mandell, et al.,* 1978; *Higgins,* 1979].

For a spacecraft, there will be approximate azimuthal symmetry if the satellite is rapidly rotating, so that it experiences only time-averaged photoemission. By rapid motion, we mean that the governing resistance/capacitance time constant is long compared to the spin period. Both models assume azimuthal symmetry around the spin axis.

As described in Section 2, the MD,MQ models can be specified by two parameters, K and $A,A2$, and we compare the models as a function of deviations from the $A,A2$ parameter lower limits. In Section 3, we describe some simple ideal solutions for the case where the satellite is represented by a thin dielectric sphere. In Section 4, we discuss the more general MD,MQ cases and compare the calculated ratio between the maximum and minimum potentials on the surface to measured ratios for eclipse to sunlight charging obtained from the LANL geosynchronous satellites. Section 5 contains a brief summary of the two sunlight charging models.

2. COMPARISON OF THE MD AND MQ CHARGING MODELS

At geosynchronous altitudes, when the ambient charge density is low, we expect the potentials outside the satellite to approximately satisfy the Laplace equation. If spherical coordinates are used, the method of separation of variables can be employed to split Laplace's equation into three ordinary differential equations; one for the radius r, polar angle θ, and azimuth angle ϕ. In the case of a spherical satellite with azimuthal symmetry (no ϕ dependence), the outside potentials can be expanded in the form [Schwartz, 1972].

$$V(r,\theta) = \sum \frac{a_n P_n(\theta)}{r^{n+1}} \tag{1}$$

where the sum is over n and goes from zero to infinity. The a_n are constant coefficients which depend on the case considered, and the $P_n(\theta)$ are the Legendre polynomials of order n. In this report, we will consider only the first three terms in the expansion.

It is convenient to factor out the monopole term so that we can write

$$V(r,\theta) = \frac{K}{r}\left(1 + \frac{A1\,P_1(\theta)}{r} + \frac{A2\,P_2(\theta)}{r^2}\right) \tag{2}$$

where K is the monopole coefficient and $A1$ and $A2$ are the strengths relative to the monopole.

If we take $r = 1$ on the satellite surface, the potentials reduce to

$$V(\theta) = V(1,\theta) = K\,(1 + A1\,P_1(\theta) + A2\,P_2(\theta)) \tag{3}$$

The MD model corresponds to $A2 = 0.0$ and the MQ model to $A1 = 0.0$. The models thus have two parameters; K and $A1$ for MD, or $A2$ for MQ. In typical charging cases, K is negative and in the KV range. The $A1/A2$ parameter sets the radius and height of the potential barrier that forms outside the sphere.

To find the radius of the potential barrier, we take

$$\frac{d\,V(r,\theta)}{dr} = 0.0 \tag{4}$$

2

which gives, using Eq. (2)

$$\frac{-K}{r^2}\left(1 + \frac{2\,A1\,P_1(\theta)}{r} + \frac{3\,A2\,P_2(\theta)}{r^2}\right) = 0.0 \qquad (5)$$

For the MD case, we get from Eq. (5) that the radius RB of the barrier is

$$RB = -2\ A1\,P_1(\theta) = 2\ A\cos(\theta) \qquad (6)$$

where we define $A = -A1 > 0$ (our notation agrees with a previous treatment [*Besse and Rubin*, 1980]; if $A1$ were > 0, then the Sun would be at *180* degrees instead of at *0*). In the same way, for the MQ model, we get

$$RB = \sqrt{-3\ A2\ P_2(\theta)} = \sqrt{-\frac{3}{2}\ A2\ (3\cos(\theta)^2 - 1)} \qquad (7)$$

Let us now consider the barrier radius as a function of θ. We assume the Sun angle is specified by the point where the radial barrier extends farthest out from the sphere surface. For the MD model, this condition gives $\theta = 0$. The MQ model is a bit more complicated, but one can see that RB will be maximum when $-P_2(\theta)$ is a maximum, which gives $\theta = 90\ degrees$.

The condition that the barrier lie outside of the sphere at the model Sun angle leads to lower limits on the $A/A2$ parameter. Hence, imposing the condition $RB > 1$ for the MD model at $\theta = 0$ yields $A > 1/2$, and imposing it for the MQ model at $\theta = 90$ gives $A2 > 2/3$.

The barrier radius RB at the model Sun angle is shown in Figure 1. Here, in order to facilitate comparison of the two models, we have introduced the variable Δ, with range (0, 1/2), which represents the deviation of either A or $A2$ from its lower limit, i.e.

for the MD model, $\Delta = A - 1/2$, with A range (1/2, 1),
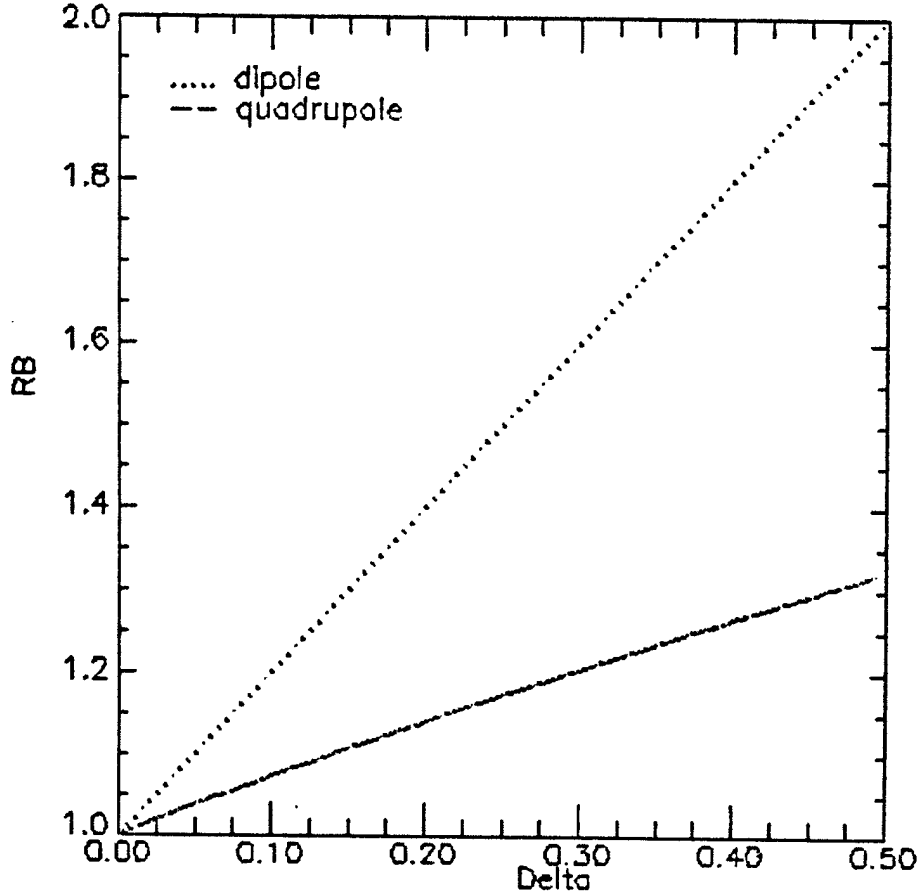for the MQ model, $\Delta = A2 - 2/3$, with $A2$ range (2/3, 7/6).

3

Figure 1. Barrier Radius Versus Δ.

From the plot, we see that the MQ model barriers form relatively closer to the sphere surface than for the MD model.

The actual height, VB, of the barrier can be obtained from

$$VB = V(RB, \theta) - V(1, \theta) \tag{8}$$

where θ is the angular location of the barrier. The barrier height at the model Sun angle, normalized to K, is plotted in Figure 2 against the deviation Δ. It can be seen that, as VB / K goes to zero, the parameters A and $A2$ approach their lower limits.
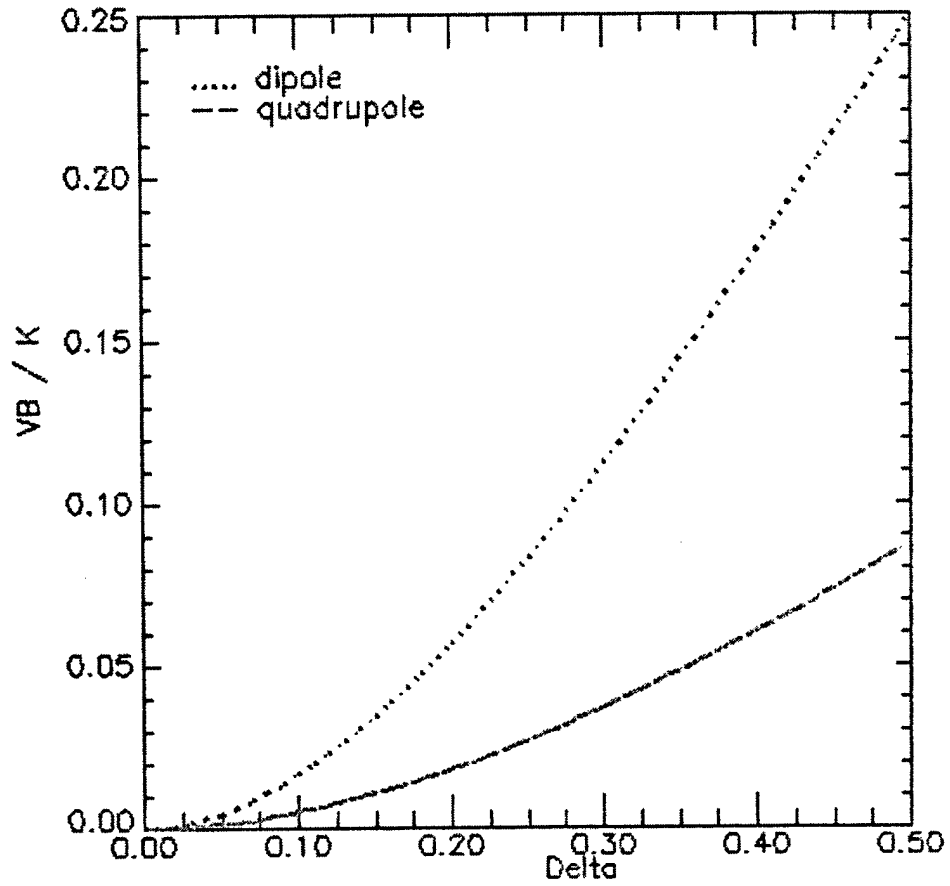
Figure 2. Barrier Potential/K Versus Δ.

The maximum angular half width of the barrier, with respect to the Sun angle, can be obtained from the models by using the condition $RB = 1$, and this is shown in Figure 3. The barriers are confined to relatively smaller angular regions for the MQ model.
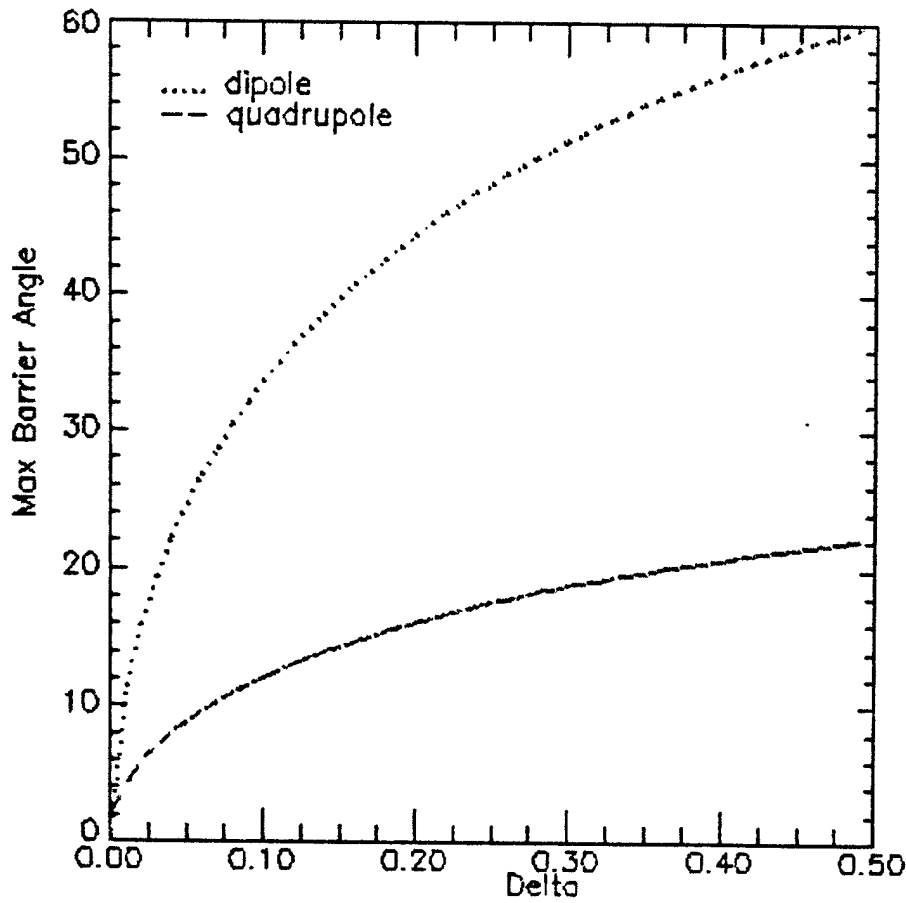
Figure 3. Maximum Barrier Angle Versus Δ.

The maximum and minimum surface potentials in the models are, from Eq. (3), simple linear functions of the parameters. In the MD model, the highest surface potential is on the shade side and the lowest on the sunlit side

$$V_{max} = V(180) = K(1 + A) \tag{9}$$

$$V_{min} = V(0) = K(1 - A) \tag{10}$$

whereas with the MQ model the high potentials are at the poles of the sphere and the low at the belly-band

$$V_{max} = V(0) = V(180) = K(1 + A2) \tag{11}$$

6

$$V_{min} = V(90) = K\left(1 - \frac{A2}{2}\right) \tag{12}$$

The high and low potentials for the models, normalized to K, are shown in Figure 4.
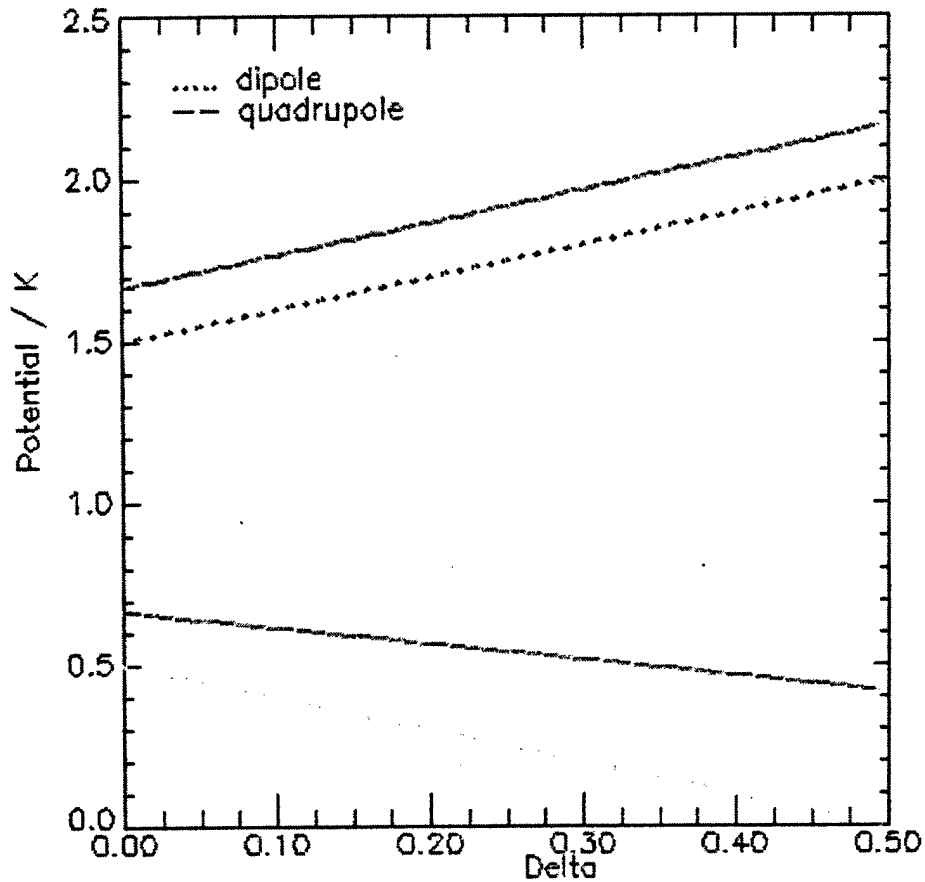
Figure 4. High and Low Potentials Versus Δ.

A quantity of further interest, for comparison with measurements, is the ratio V_{max} / V_{min}, which is shown in Figure 5. The minimum ratio for the MD model occurs at the lower limit for A

$$ratio = \frac{(1+A)}{(1-A)} = \frac{\frac{3}{2}}{\frac{1}{2}} = 3.0 \qquad (13)$$

and for the MQ model it is at the lower limit for *A2*

$$ratio = \frac{(1+A2)}{\left(1-\frac{A2}{2}\right)} = \frac{\frac{5}{3}}{\frac{2}{3}} = 2.5 \qquad (14)$$

Figure 5. High/Low Ratios Versus Δ.

It is evident that the ratios are slightly larger for the MD model at low Δ, and the difference increases with Δ. For co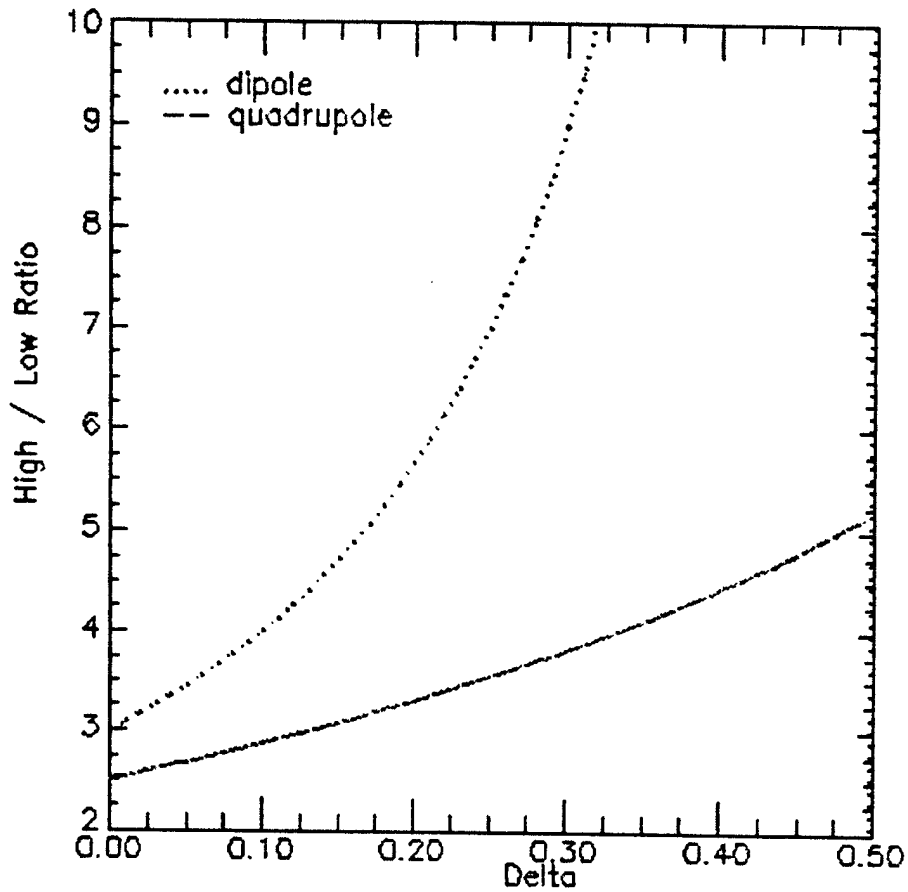mparison, in the MD model, the lower limit ratio between the maximum potential to that on the belly-band (equal to K) is $1 + A = 1.5$.

Color contour plots for the two models, at $\Delta = 0.1$, are shown in Figures 6 and 7. The variable plotted is the model potential, normalized to K. In the figures, the angle $\theta = 0$ points to the top. One can see from the plots how a potential barrier arises due to encroaching high fields from elsewhere on the surface. In the MD model, the high fields come from the shade side (bottom) and make a barrier on the sunlit side (top). In the MQ case, the high fields come from the top and bottom, and combine to make a barrier at the belly-band.
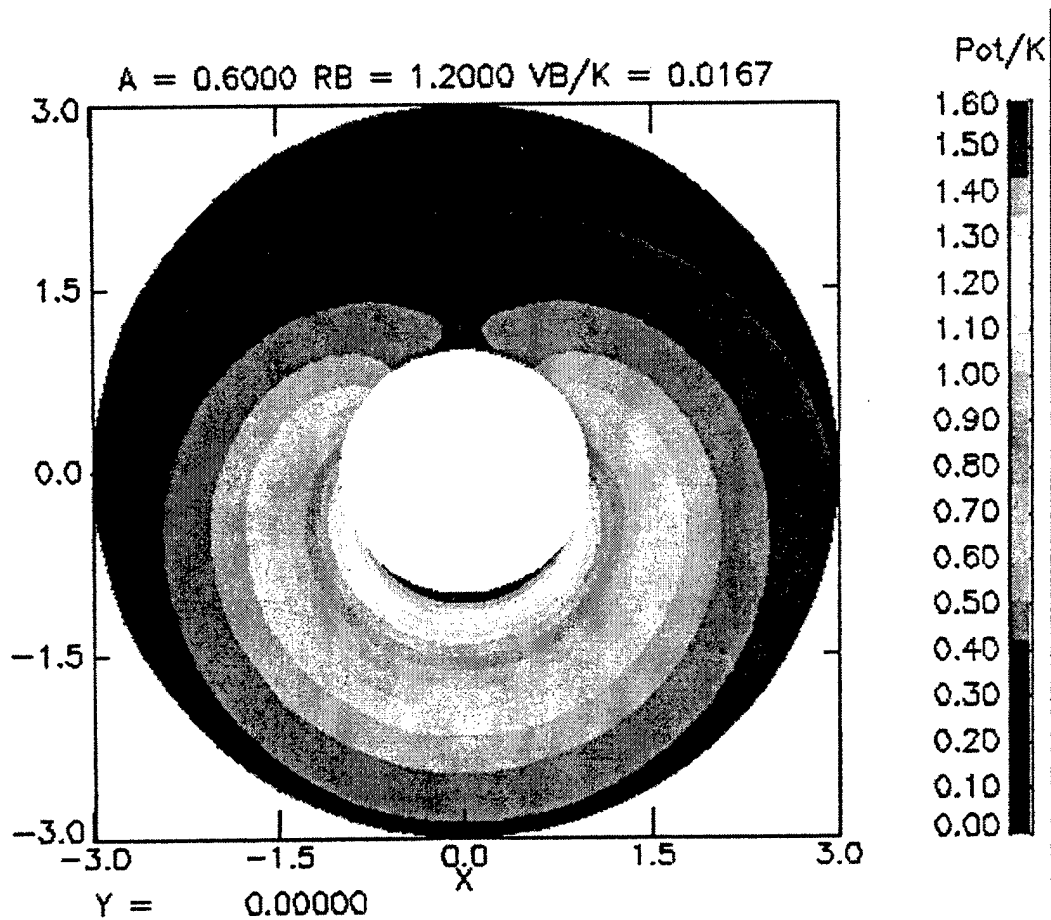

Figure 6. The Monopole-Dipole Model.
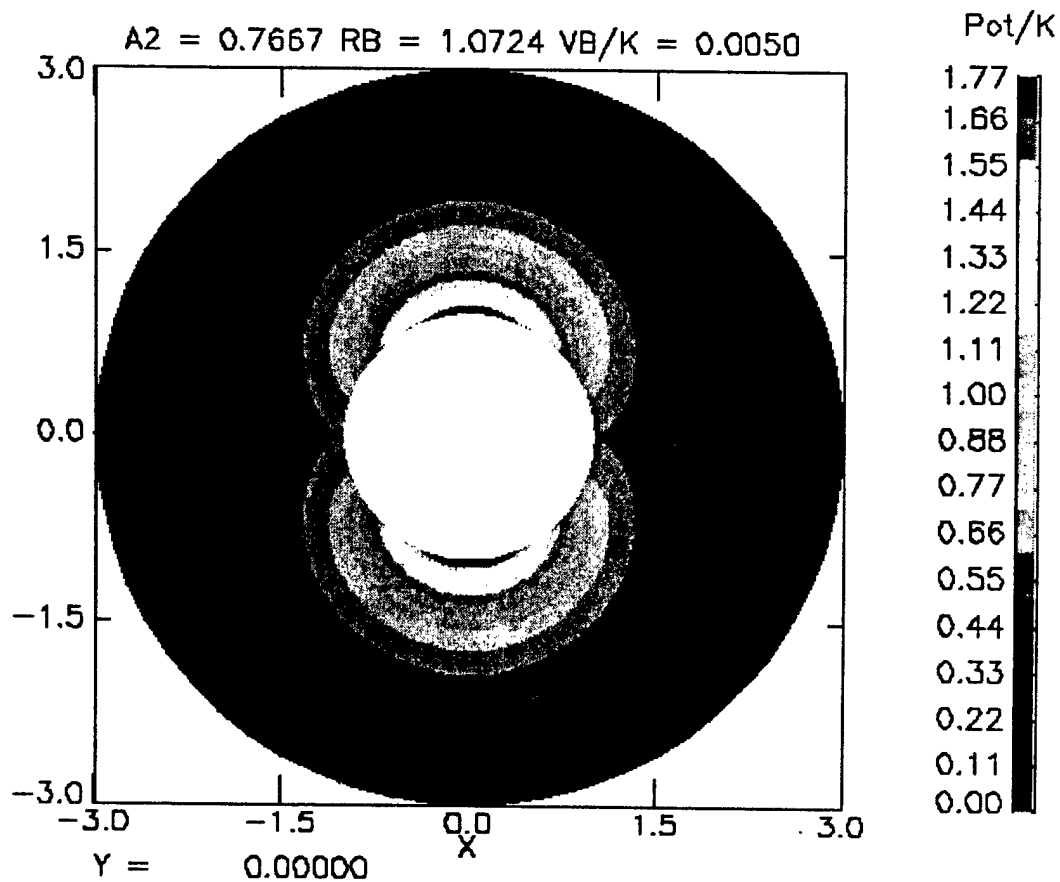
Figure 7. The Monopole-Quadrupole Model.

We summarize the main differences between the MD and MQ models:

- the Sun direction differs by 90 degrees.
- the lower limits for the A and $A2$ parameters are not the same.
- in the MD model the potential barrier forms at the pole (sunlit side), whereas in the MQ model it occurs at the belly-band.
- in the MD model the maximum potential occurs at the back (shade side), while in the MQ model the maximums occur at the poles.
- the ratios of maximum to minimum surface potential are slightly different.

These elementary models provide an intuitive look at the physics of sunlight charging, which is often absent in complex computer simulations.

10

3. IDEAL MODELS: CHARGING OF A DIELECTRIC SPHERE

It is possible to investigate these models further by considering the simple case where the sphere is covered by a thin dielectric layer connected to ground. Here, we divide a unit sphere of area $S=4\pi$ into azimuthal sectors with areas

$$dS = 2\pi \sin(\theta)\, d\theta \tag{15}$$

A lumped circuit model can be configured and we can write for each sector surface element

$$\left(V(\theta) - Vg\right)\frac{\sigma}{d}\, dS = I(\theta) = J(\theta)\, dS \tag{16}$$

where σ is the material conductivity, d is the thickness, and Vg is the ground potential underlying the dielectric. $I(\theta)$ is the net current through the material, including secondaries and backscatter, and $J(\theta)$ is the net current density.

If we have current balance to the sphere, then we can write

$$\sum I(\theta) = \sum J(\theta)dS = 0.0 \tag{17}$$

where the sum is over the sectors. Using the current balance condition, we get from Eq. (16)

$$Vg = \sum V(\theta)\frac{dS}{S} \tag{18}$$

i.e., the ground potential is given by the area weighted average over the sectors. If the surface potentials are specified by the MD or MQ models, we can substitute Eq. (3) in Eq. (18) to get

$$Vg = \sum K\left(1 + A1\, P_1(\theta) + A2\, P_2(\theta)\right)\frac{dS}{S} \tag{19}$$

and replacing the sum by an integral, valid as the number of sectors becomes large, we find

11

$$Vg = K \frac{\left(\int dS + A1 \int P_1(\theta) \, dS + A2 \int P_2(\theta) \, dS\right)}{S} = \frac{K(S+0+0)}{S} = K \qquad (20)$$

Here we have used a result for the Legendre polynomials that the integral over the total surface is zero when $n > 0$ (see Appendix).

The actual numerical values of the net current density to the sectors would depend, from Eq. (16), on the model parameters plus the dielectric properties

$$J(\theta) = \left(A1 \ P_1(\theta) + A2 \ P_2(\theta)\right) K \frac{\sigma}{d} \qquad (21)$$

and the net currents $I(\theta)$ would further depend on the sector areas. The ideal net current density $J(\theta)$ for the MD case, would be proportional to $P_1(\theta) = cos(\theta)$ (taking $A1,K$ negative). Thus, positive J would appear at the north pole $(\theta=0)$, and negative at the south pole $(\theta=180)$, with zero J at the belly-band. Interpreting the negative J as net incoming electrons, we see that there would be electron flow through the sphere from south to north. For the MQ case, the ideal net current density would be proportional to $-P_2(\theta)$ (again K is taken negative). This function is symmetric about $\theta = 90$, with negative J appearing at the poles, and positive J at the belly-band. This could be interpreted as due to electrons entering at the poles and exiting at the belly-band. In both models, the current balance is achieved by electrical flow through the satellite. This is a prototypical situation which occurs also in the non-ideal charging cases when dark and sunlit surfaces are conducting and connected.

We see that for these ideal models, the current balance is due to the Legendre terms, and is therefore independent of $A1/A2$. Hence, we don't need a potential barrier to help create the current balance, and we can replace $A1/A2$ by the model lower limit. We note that the current balance would hold for any number of Legendre polynomial terms $(n > 0)$.

4. NON-IDEAL CHARGING AND COMPARISON WITH LANL DATA.

In a real charging case, the spacecraft body probably would not be a sphere, there would not be exact azimuthal symmetry, and the surface materials and underlying electrical connections could be anything. In the above analysis, only the current balance condition would hold rigorously. But we might still expect that the potentials outside the satellite would be approximately Laplacian and that a potential barrier would form to suppress photoemission. Computer simulations with more complex satellite models have indicated the occurrence of this effect [*Mandell, et al.,* 1978; *Rubin, et al.,* 1979].

For a spherical satellite that was approximately azimuthally symmetric, the net surface current density, which would be a complicated function of the environment, the surface potentials, and the materials properties, could be expanded in terms of the Legendre polynomials

$$J(\theta) = \sum J_n P_n(\theta) \tag{22}$$

where the sum is over n, the J_n are fit coefficients, and θ is again the polar angle. Because of the properties of the Legendre polynomials, only the $n = 0$ term in the expansion would contribute to the total spacecraft current, integrated over all sectors, i.e.,

$$\int I(\theta) = \sum J_n \int P_n(\theta) \, dS = 4\pi J_0 \tag{23}$$

We expect that a potential barrier would be set up, such that J_0 goes to zero. Photoemission would occur at all sectors that were exposed to the Sun, with intensity proportional to the cosine of the Sun to sector angle. The emitted photoelectrons would fall to the sunlit pole (MD model) or to the belly-band (MQ model) and experience the radial barrier. A small fraction would escape the barrier and balance the net current to other parts of the satellite. The fraction of photoelectron flux escaping a linear barrier of height VB is given by

$$f = \exp\left(\frac{-VB}{Tp}\right) \left(1 + \frac{VB}{Tp}\right) \tag{24}$$

where Tp is the photoemission temperature (~2eV). Because the photoelectron flux is typically much larger than the electron or ion-induced current densities at geosynchronous orbits, the barrier potential VB would rise to a few times Tp. But if VB is small compared to other potentials in the problem (VB would be typically less than 10 Volts and K can be in the KV range), the model parameters $A,A2$ would not depart much from their lower limits, as is shown in Figure 2. Thus, the ratio V_{max} / V_{min} would remain fairly close to its value at the lower limits (~3.0), as shown in Figure 5.

With the MD and MQ models in mind, we have looked at the Los Alamos National Laboratory (LANL) geosynchronous satellite charging data, obtained from their network site [*cdaweb.gsfc.nasa.gov*, 2002]. We did not expect to see front to back or top to belly-band potential variations in the LANL data because their detectors are located at the middle of the satellites. The fact that the charging potential in sunlight was largely independent of the spin phase [*Private communication, S. Lai*, 2002] suggests that the satellites were in a rapid rotation state (the spin period was ~10 seconds). The spin axis on the satellites was constrained to point at the Earth center. Thus, at the equinoxes, when the spacecraft passed into eclipse, it would probably be near to the MD model. In general, depending on the time, it would be somewhere between the two models.

To improve their statistics, the LANL charging data was determined based on the spin-averaged energy spectra for ions and electrons. The LANL charging potential could be identified from the channel occupied by low-energy ambient ions that were accelerated through the sheath. When there was a valid ion line (sometimes it was absent and an iterative scheme was used to identify the charging) the spacecraft potential was estimated from minus the ion line energy. This procedure leads to quantized charging levels, making the comparison with analysis less direct.

The LANL database has files composed in the National Space Science Data Center (NSSDC) common data format (CDF). CDF utilities [nssdcftp.gsfc.nasa.gov, 2002] were used to convert the files from CDF into ASCII text, and UNIX scripts were run to extract selected data from the spring and fall equinox periods. The selected LANL data is shown in Figures 8 to 17, and includes both eclipse and sunlight charging voltages for March and September periods, and for five different satellites. In the plots, the upper data is due to eclipse charging, and the lower data represents sunlight charging. The horizontal axis is the electron temperature in eV.

Note that when the actual ratios observed are eclipse to sunlight charging, the values would be somewhat larger than the calculated V_{max} / V_{min} ratio because the eclipse charging potentials should be equal or greater than the V_{max} from the models. On the other hand, the calculated ratio of the maximum potentials to those on the belly-band are less than three at the lower limits of the models. For comparison with experiment, we use a ratio of three.

The curves shown in the plots were generated as follows:
- first a fit was made to the sunlight-charging data, using the LANL 97-A satellite data for September.
- this fit curve was included in the other plots (lower curve)
- a second curve, at three times the background fit, was added to the plots (upper curve).

It is observed that the upper curve falls within the span of the measured quantized potential levels in all ten cases. This suggests a connection with the above models, where a ratio of about three is a characteristic value. A more detailed comparison with LANL data would require knowledge of the satellite body geometry, the surface material properties, and the electrical configuration.
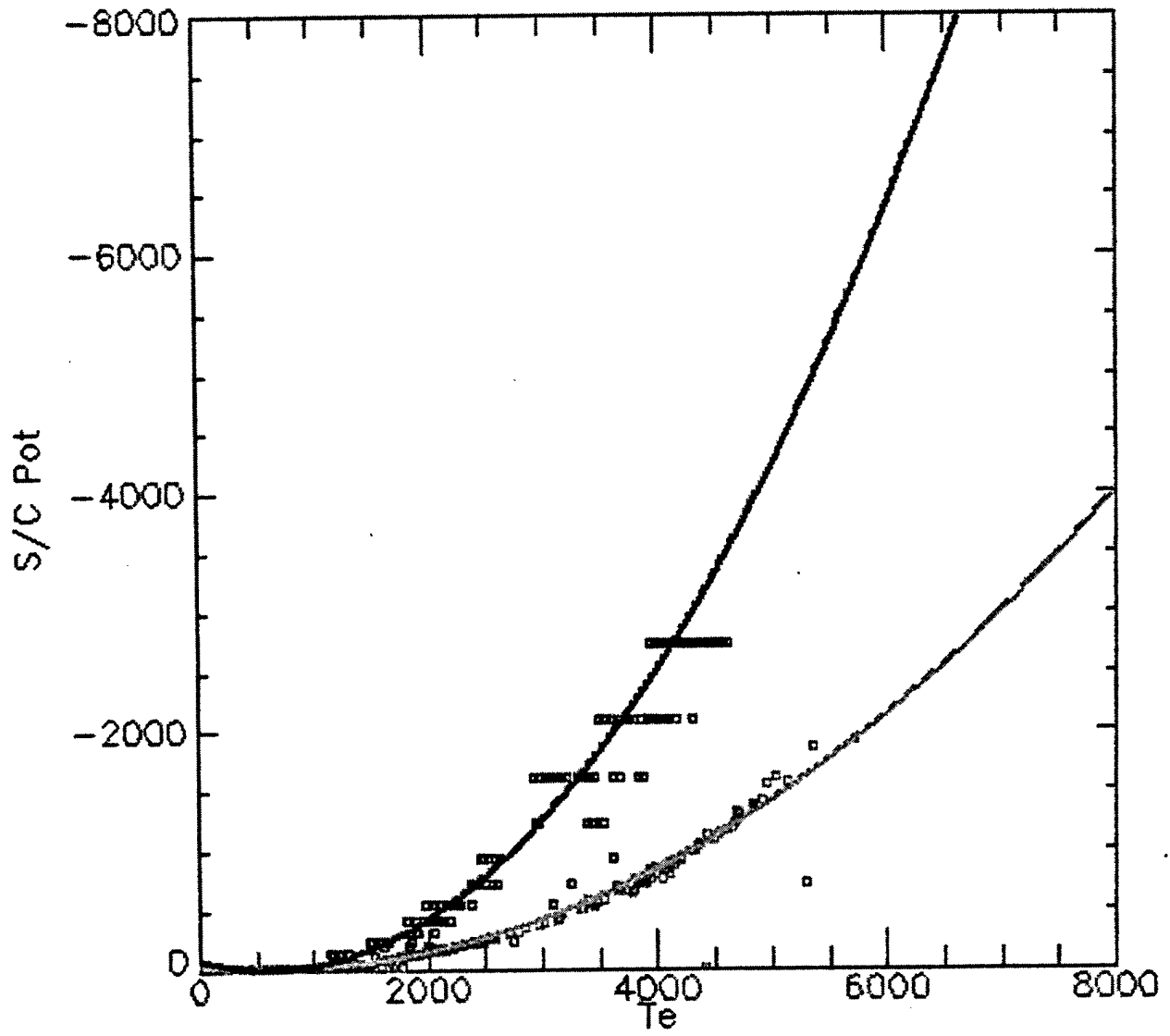
Figure 8. LANL Eclipse and Sunlight Charging.
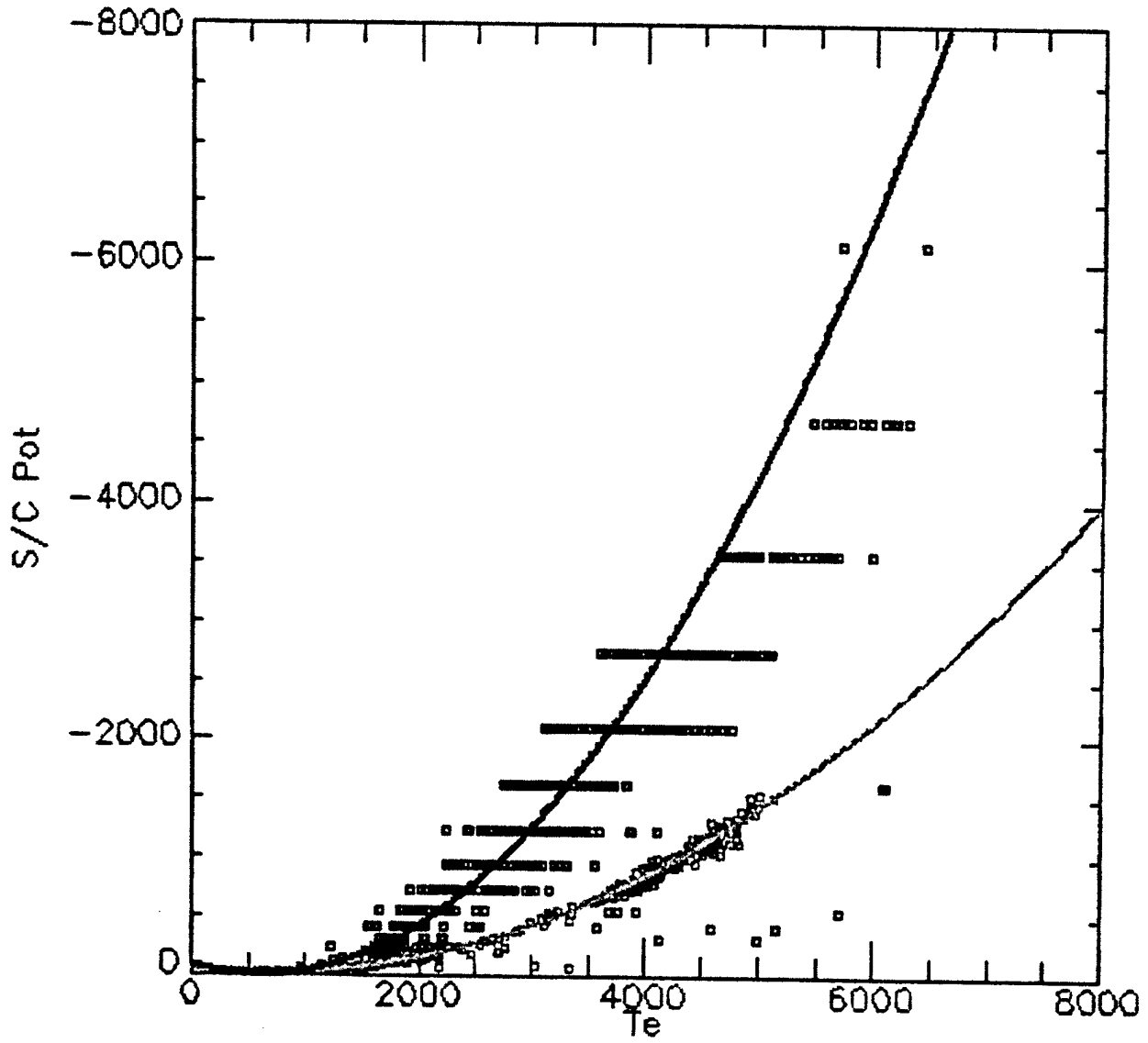LANL-1997A: Mar 13 to 27, 1998-1999

Figure 9. LANL Eclipse and Sunlight Charging.
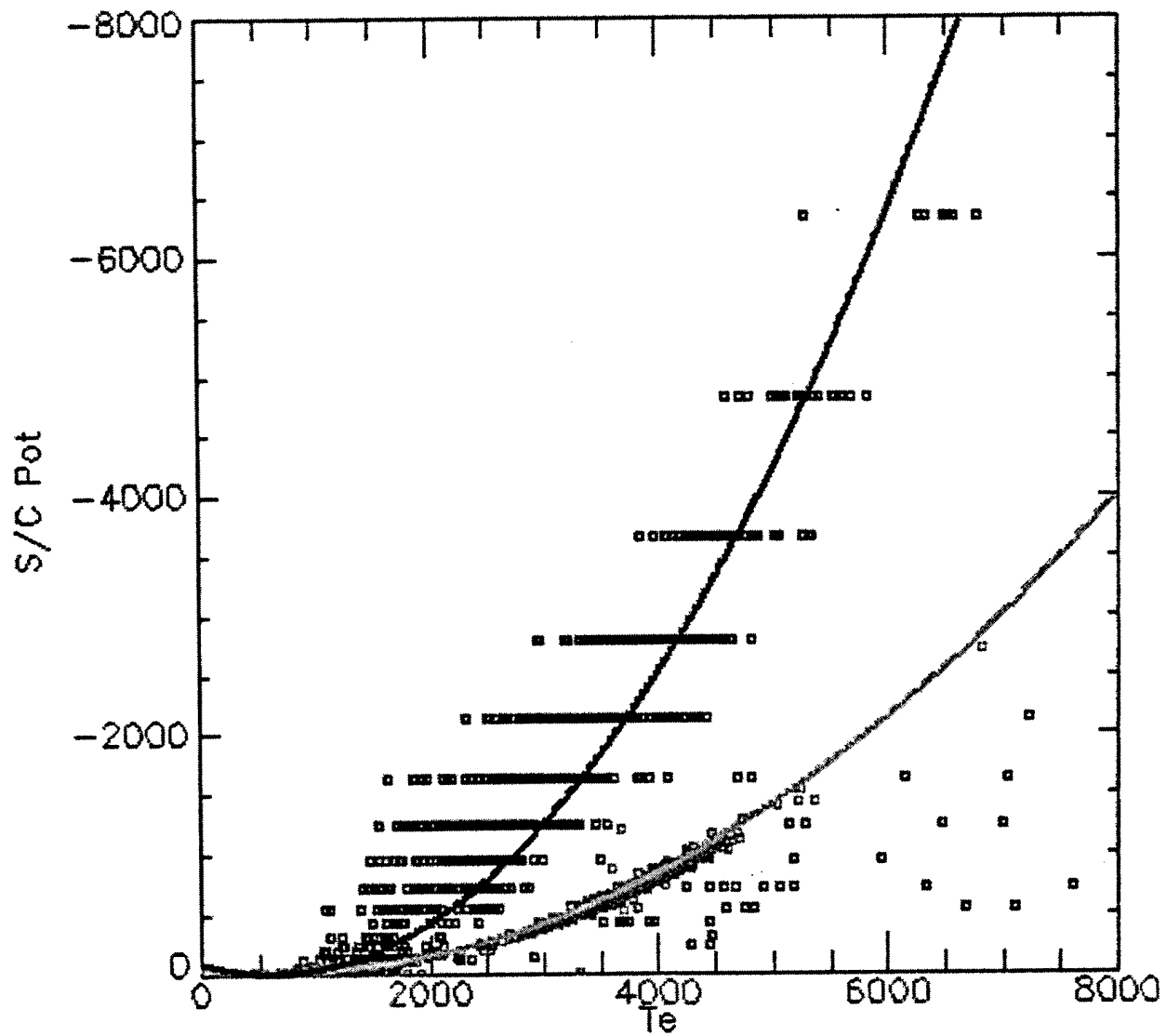LANL-1997A: Sep 14 to 28, 1997-2001

Figure 10. LANL Eclipse and Sunlight Charging.
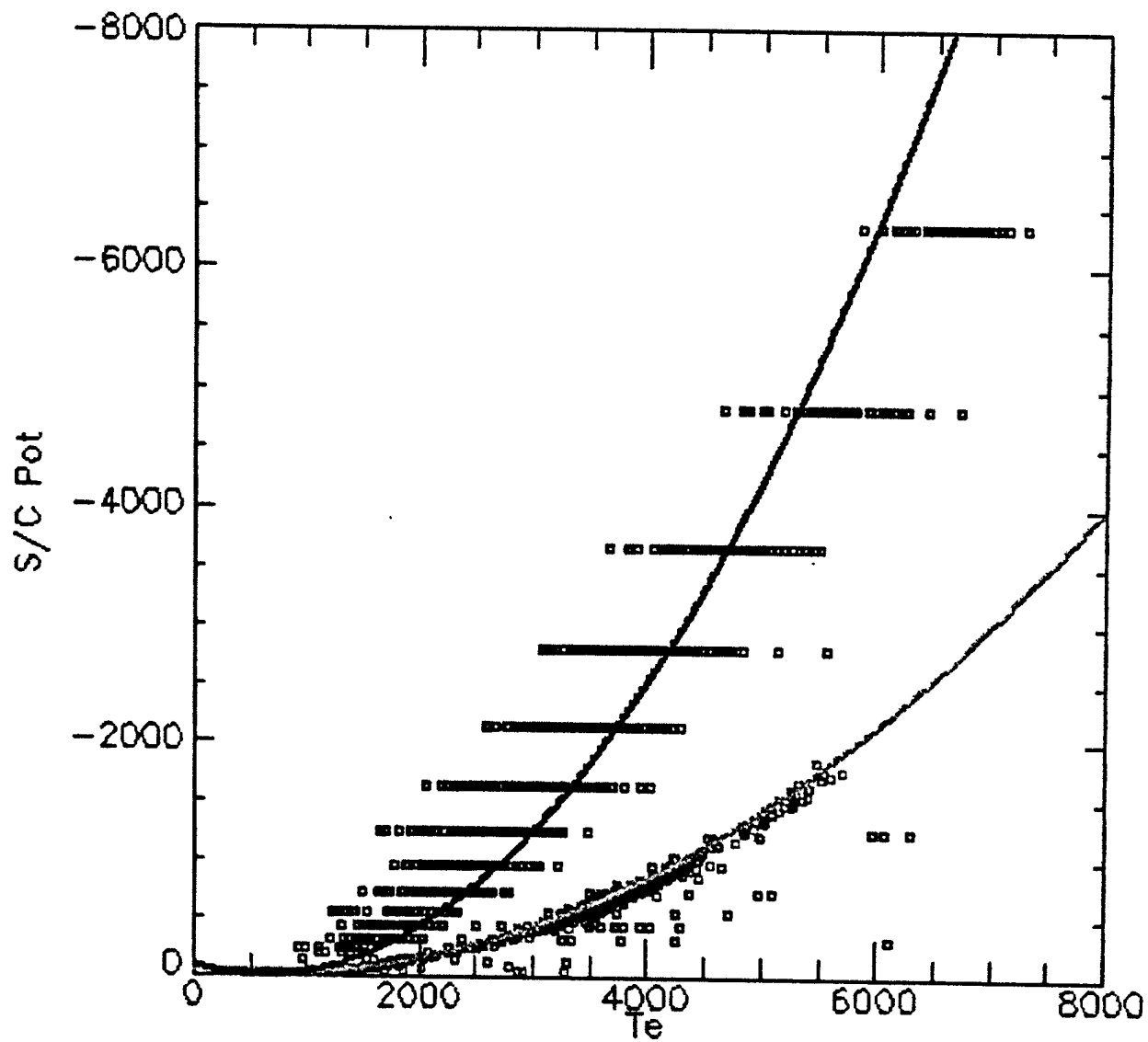LANL-1994-084: Mar 13 to 28, 1996-2001

Figure 11. LANL Eclipse and Sunlight Charging.
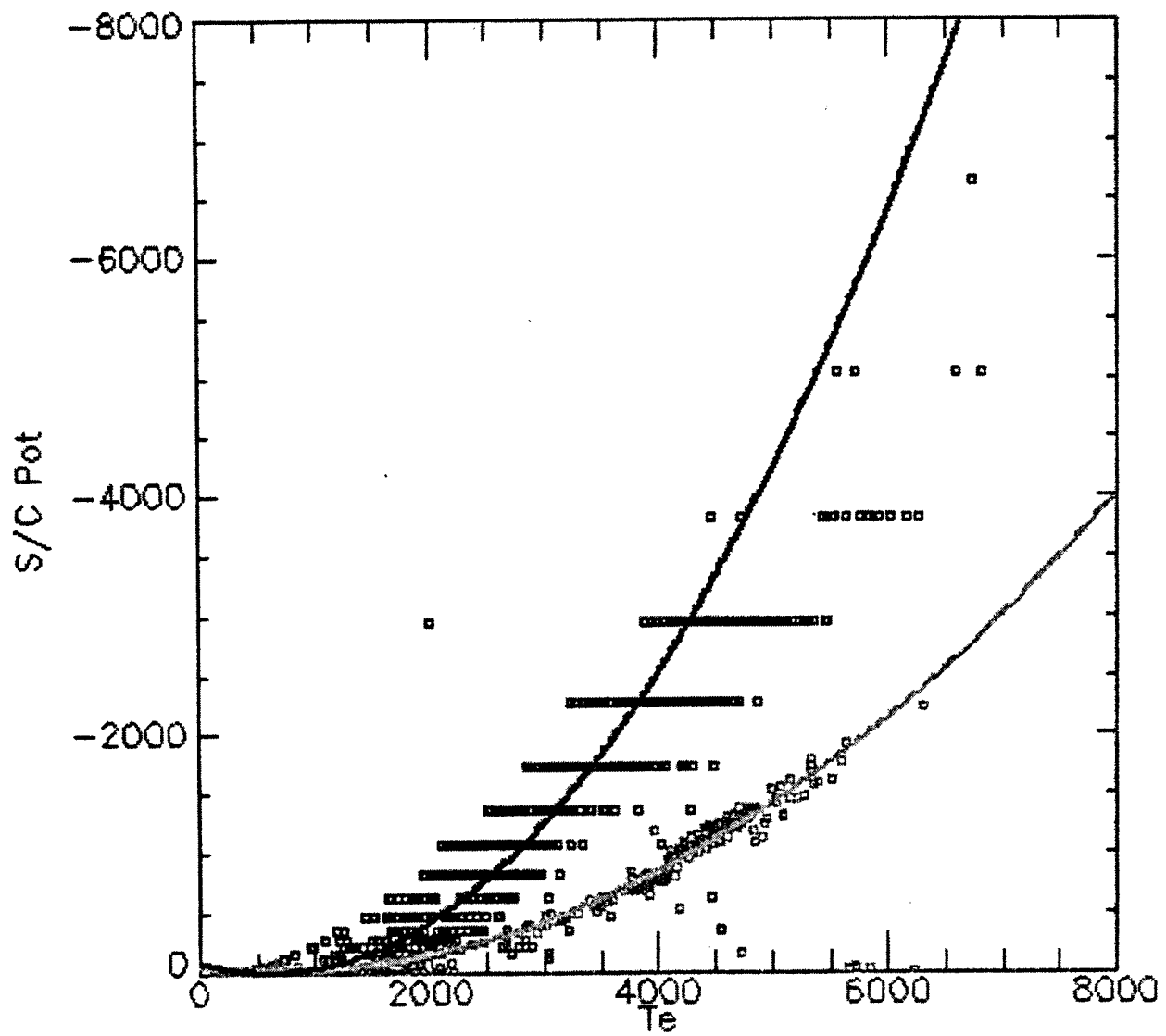LANL-1994-084: Sep 14 to 29, 1996-2001

Figure 12. LANL Eclipse and Sunlight Charging.
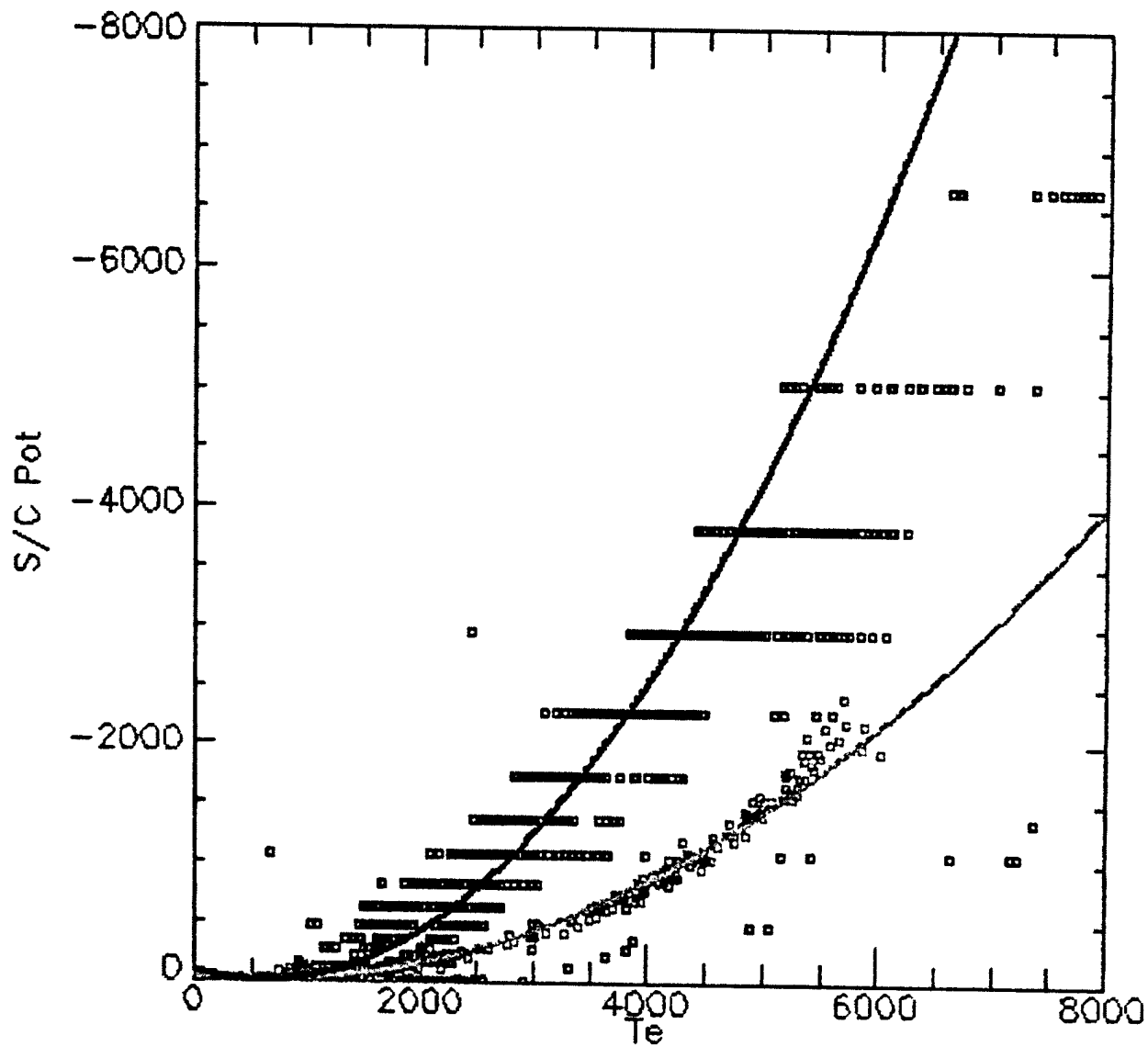LANL-1991-80: Mar 13 to 28, 1994-2001

19

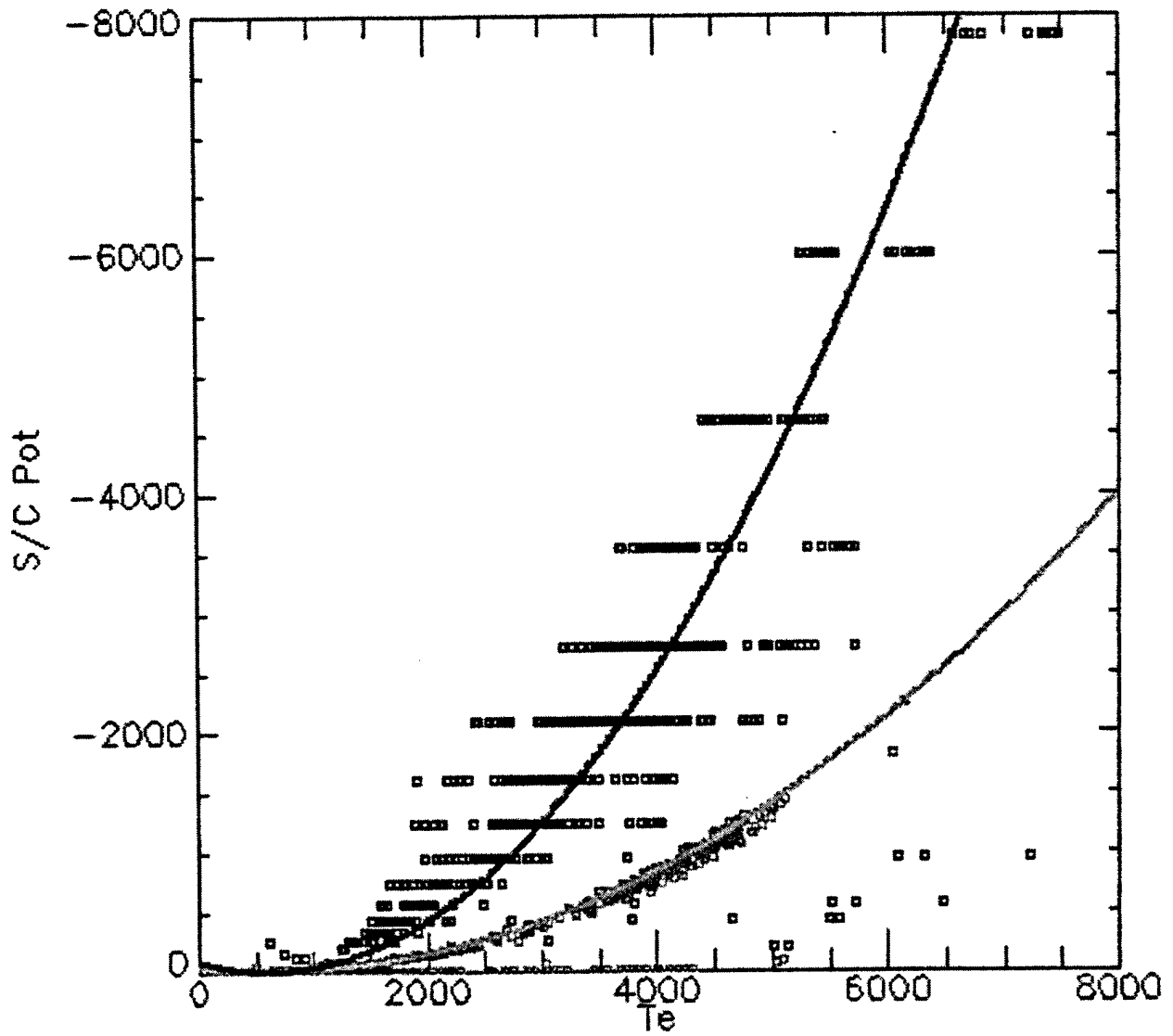**Figure 13.** LANL Eclipse and Sunlight Charging.
LANL-1991-80: Sep 14 to 29, 1994-2001

20

Figure 14. LANL Eclipse and Sunlight Charging.
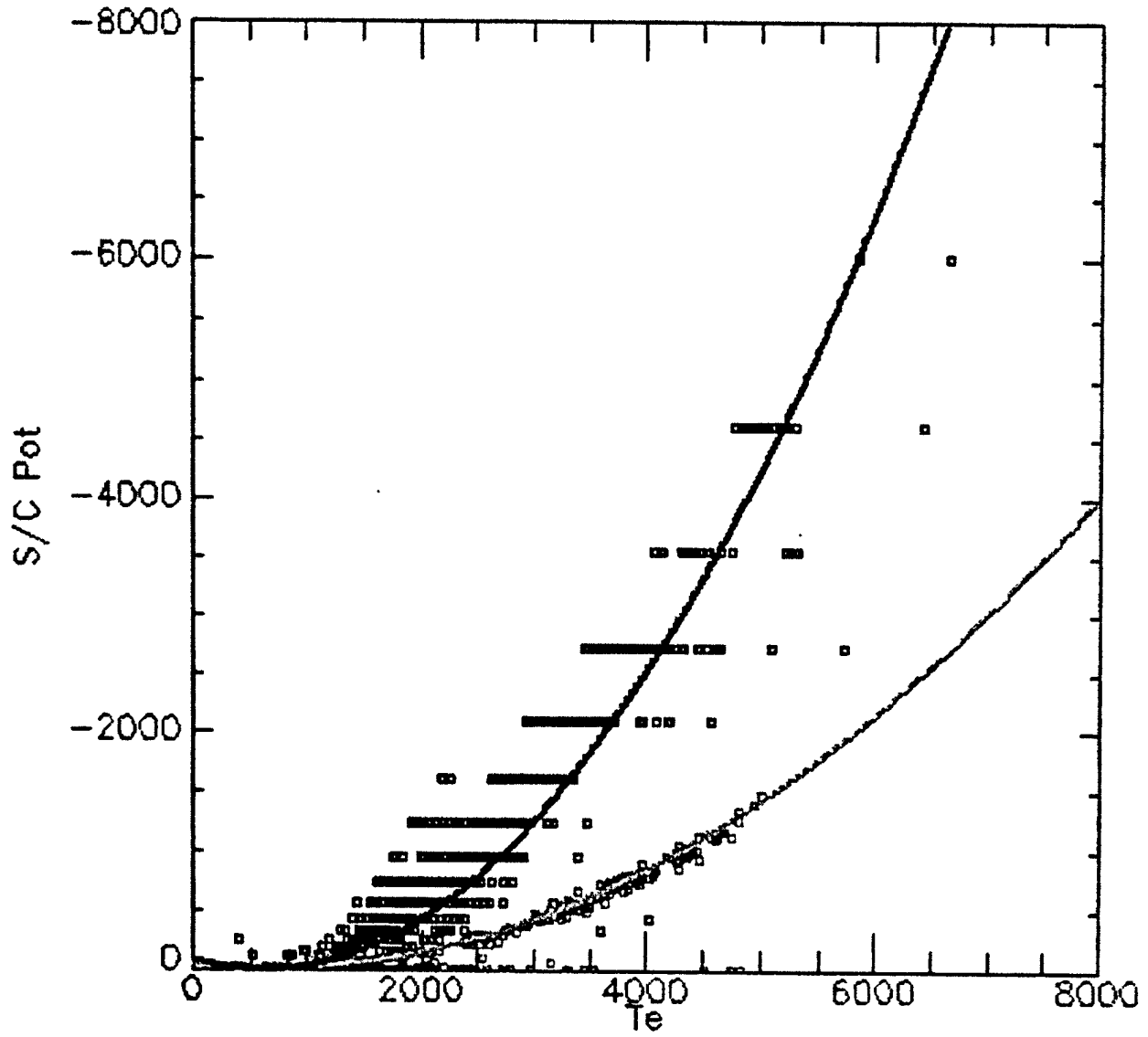LANL-1990-095: Mar 12 to 27, 1993-2000

21

Figure 15. LANL Eclipse and Sunlight Charging.
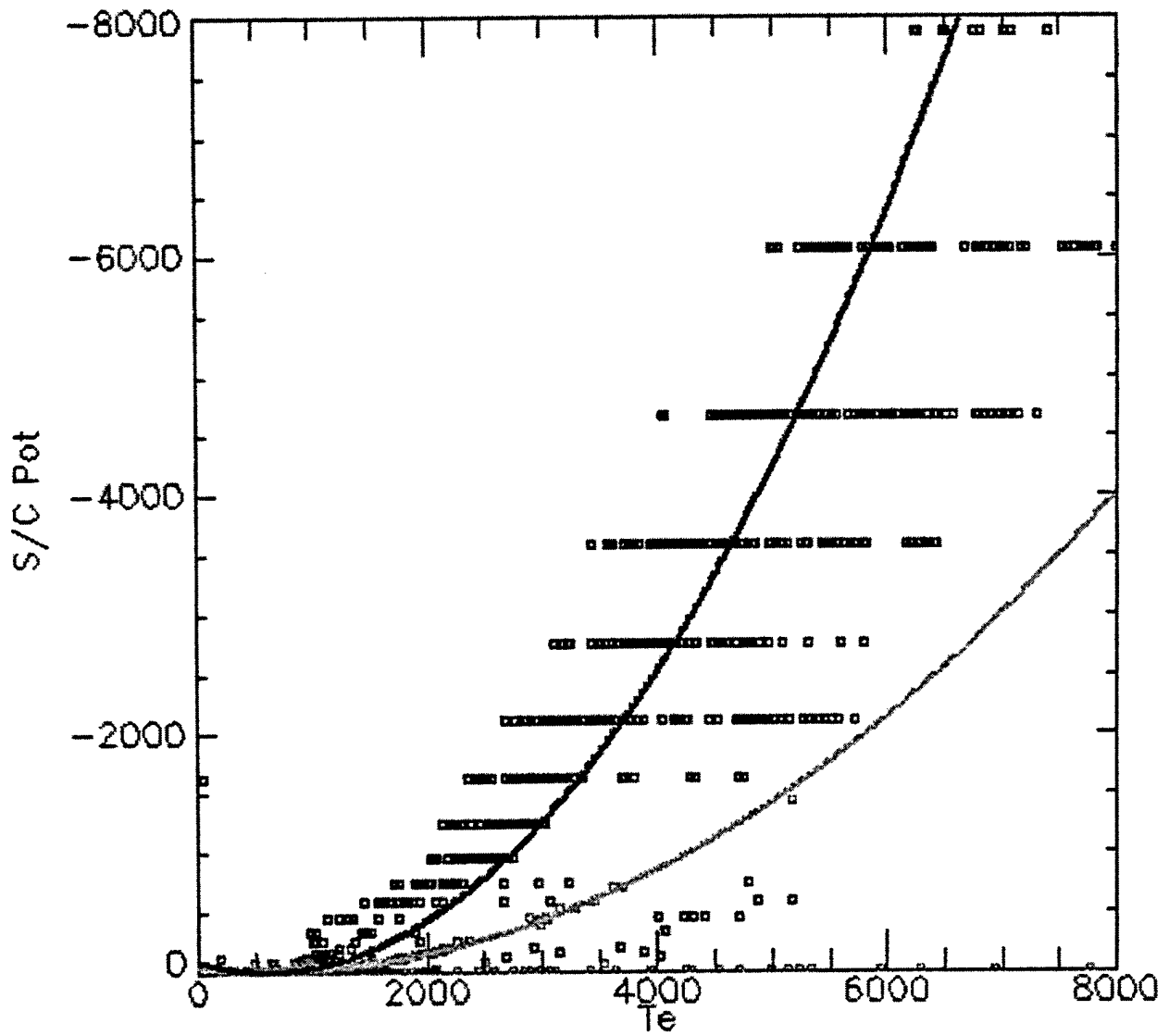LANL-1990-095: Sep 14 to 29, 1993-2001

Figure 16. LANL Eclipse and Sunlight Charging.
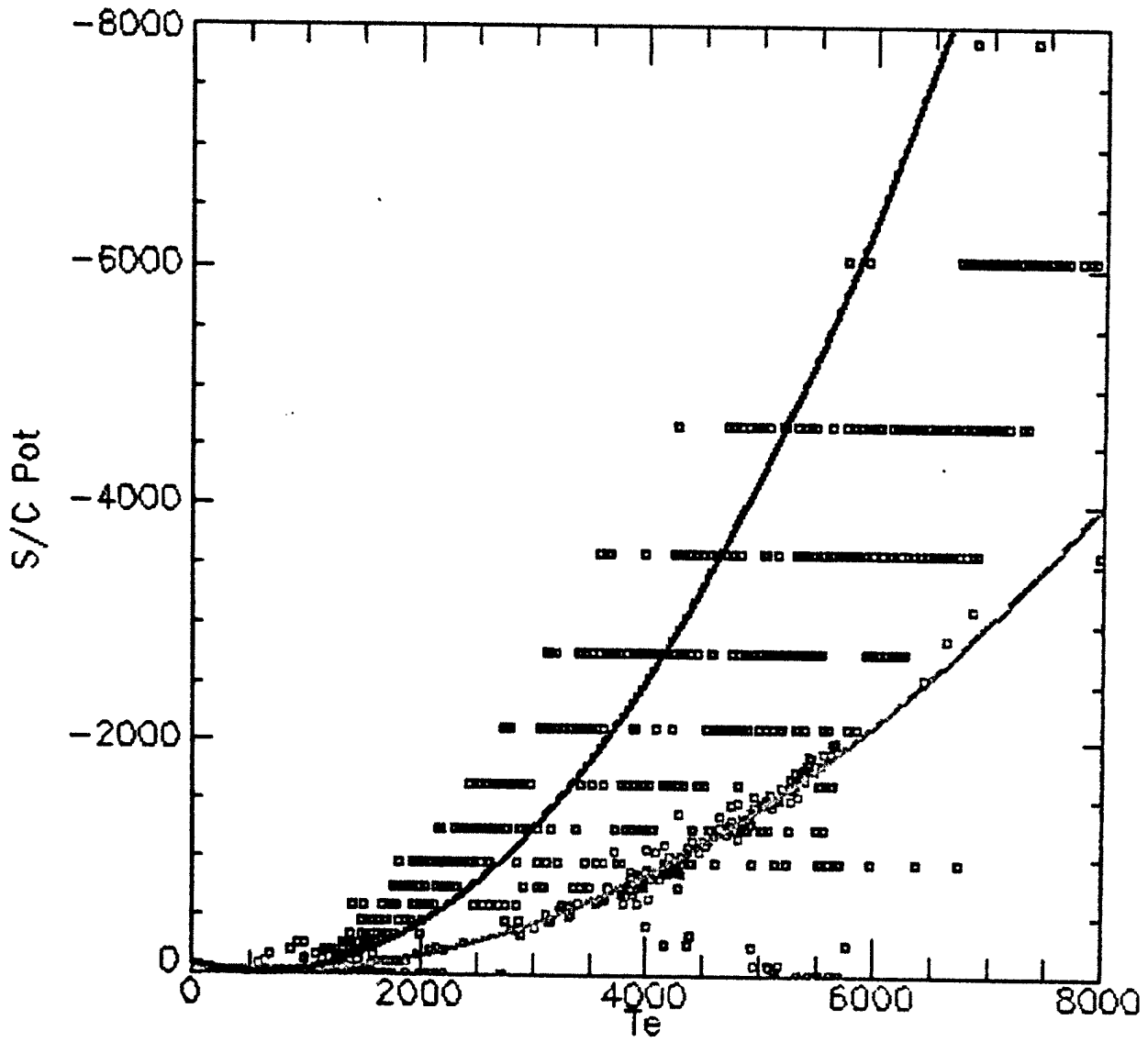LANL-1989-046: Mar 13 to 28, 1993-2001

23

Figure 17. LANL Eclipse and Sunlight Charging.
LANL-1989-046: Sep 13 to 28, 1993-2000

24

5. SUMMARY

The potentials exterior to a spacecraft in geosynchronous orbit would be approximate solutions to the Laplace equation when the ambient charge density is low. A rapidly spinning satellite would have approximate azimuthal symmetry around the spin axis, due to revolution time averaging. In spherical coordinates, an azimuthally symmetric spherical object will have a Laplace solution for exterior potentials given by a product expansion over inverse powers of the radius times a Legendre polynomial. The lowest order Legendre polynomial corresponds to the monopole term, the next term represents a dipole, and the third gives the quadrupole. The monopole-dipole combination represents a satellite with the spin axis pointed at the Sun, and the monopole-quadrupole solution corresponds to a satellite with the Sun at right angles to the spin axis. Both of the models set up a potential barrier to suppress escaping photoelectrons at the sunlit surfaces, so that current balance to the satellite can be achieved. In the case of the monopole-dipole model, the barrier forms at the sunlit side pole, and for the monopole-quadrupole model, it forms at the belly-band. When the barrier potential is much less than the charging potentials, the model parameters $A, A2$ should be near to their lower limits. For both models, at these lower limits, the ratio of the highest to the lowest potential on the satellite surface is about three. An inspection of the measured eclipse to sunlight charging potentials on the LANL geosynchronous satellites shows a ratio that is compatible with three.

REFERENCES

Besse, A. and A. Rubin, A simple analysis of spacecraft charging involving blocked photoelectron currents, *JGR*, Vol **85**, No. A5, 2324,2328, (1980)

cdaweb.gsfc.nasa.gov, The LANL database was obtained from the network site: cdaweb.gsfc.nasa.gov, sub-directory:/pub/istp/lanl, 2002.

Higgins, D., An analytic model of multi-dimensional spacecraft charging fields and potentials, *IEEE Trans. Nuc. Sci*, Vol **26**, 6, 5162, Dec 1979.

Lai, S., *Private communication*, 2002.

Mandell, M ., I. Katz, G. Schnuelle, P. Steen, and J. Roche, The increase in effective photocurrents due to saddle points in electrostatic potentials near differentially charged spacecraft, *IEEE Trans. Nuc. Sci,* Vol **26**, 6, 1313, Dec 1978.

nssdcftp.gsfc.nasa.gov, The NSSDC/CDF library files were obtained from the network site: nssdcftp.gsfc.nasa.gov, sub-directory:/standards/cdf/dist/cdf27/unix, 2002.

Rubin, A., K. Bhavnani, and M. Tautz, "Charging of Spinning SpaceCraft", AFGL-TR-79-0261, ADA #084087.

Schwartz, M., "Principles of Electrodynamics", McGraw-Hill, New York, 1972.

APPENDIX. A NOTE ON THE LEGENDRE POLYNOMIALS

The solution of Laplace's equation in spherical coordinates can be treated by the method of separation of variables. If the problem has azimuthal symmetry, the polar angle part is solved by the Legendre polynomials $P_n(\theta)$ where θ is the polar angle and n is the order of the polynomial. The lowest order polynomials are

$P_0(\theta) = 1$ monopole

$P_1(\theta) = cos(\theta)$ dipole

$P_2(\theta) = \dfrac{1}{2}\left(3 \cos(\theta)^2 - 1\right)$ quadrupole

The Legendre polynomials are orthogonal functions which satisfy

$$\int P_m(\theta)\ P_n(\theta) \sin(\theta)\ d\theta\ =\ 0.0 \qquad if\ n \neq m \tag{A1}$$

$$=\ \frac{2}{(2n+1)} \qquad if\ n = m$$

where the integral goes from 0 to 180. Putting $m = 0$, $P_0 = 1.0$ into this equation we get

$$\int P_n(\theta) \sin(\theta)\ d\theta\ =\ 0.0 \qquad if\ n \neq 0 \tag{A2}$$

$$=\ 2.0 \qquad if\ n = 0$$

Thus, the integral over the spherical surface is

$$\int P_n(\theta)\ dS\ =\ 2\pi \int P_n(\theta) \sin(\theta)\ d\theta \tag{A3}$$

which is zero when $n > 0$, and 4π when $n = 0$.